Available online at www.sciencedirect.com

ScienceDirect

Ceramics International 40 (2014) 1189–1194

CERAMICS INTERNATIONAL

www.elsevier.com/locate/ceramint

Synthesis of nano-crystalline $Sm_{0.5}Sr_{0.5}Co(Fe)O_{3-\delta}$ perovskite oxides by a microwave-assisted sol–gel combustion process

Liping Li, Jian Song, Qing Lu, Xiaoyao Tan*

The State Key Laboratory of Hollow Fabre Membrane Materials and Processes, Department of Chemical Engineering, Tianjin Polytechnic University, Tianjin 300387, China

Received 12 June 2013; received in revised form 1 July 2013; accepted 1 July 2013
Available online 6 July 2013

Abstract

Nano-crystalline $Sm_{0.5}Sr_{0.5}Co(Fe)O_{3-\delta}$ (SSCF) perovskite oxides were synthesized by a microwave-assisted sol–gel combustion process using glycine as the complexing agent. The properties of the resultant powder were characterized by scanning electron microscopy (SEM), thermo gravimetric-differential thermal analysis (TG-DTA), Brunauer–Emmett–Teller (BET) and X-ray diffraction (XRD) techniques. The synthesis conditions to form the perovskite phase in terms of the glycine/metal-ion molar ratio, the total metal ion concentration in the starting solution and the calcination temperature were investigated and optimized. The experimental results indicated that the glycine/metal-ion ratio should be controlled at about 2 with the starting metal ion concentration of 0.25 mol L^{-1} and the calcination temperature should be around 800 °C so as to obtain the pure perovskite structure with high economical efficiency. The overall synthesis period of perovskite oxides can be reduced significantly compared to the conventional combustion route. The partial substitution of Fe for Co cations with molar fraction higher than 0.2 could improve noticeably the stability of the perovskite against CO_2, but the calcination temperature to obtain pure perovskite phase should be increased.

Keywords: Sol–gel; Perovskite; Combustion; Microwave; Nano-crystalline

1. Introduction

Mixed ionic-electronic conducting perovskite oxides with the general formula ABO_3, where elements for the A site can be cerium, calcium, barium, strontium or various rare earth metal to form 12 coordination with adjacent oxygen ions, and the B site can be occupied by cobalt, iron or other transition metal ions, have received considerable attention in recent years due to their extensive potential applications in oxygen/hydrogen separators, membrane reactors, catalysts, gas sensors and solid oxide fuel cells [1–4]. In order to improve the ionic/electronic conductivity or the structural stability of the perovskites, the cations at A and/or B sites usually need to be partially substituted with other metal cations with different valences. For example, the cobalt-based perovskite, $Sm_{0.5}Sr_{0.5}CoO_{3-\delta}$ (SSC) possesses extremely high electrical conductivity and rapid oxygen surface exchange kinetics at elevated temperatures, and has become one of the most promising cathode materials for the intermediate temperature solid oxide fuel cells (IT-SOFCs) [5–7]. In order to suppress the lattice expansion of the SSC perovskite for more applicability, the Co ions could be partially substituted with other ions such as Ce^{4+}, Mn^{2+} or Fe^{3+} although the doping would lead to the loss of electrical conductivity [8,9].

It is well known that the synthesis method plays an important role in the properties of the resultant ceramic oxides [2]. Nowadays a variety of methods have been developed to prepare mixed conducting perovskites such as the solid state reaction route, the spray pyrolysis and the sol–gel combustion technique etc. Each synthesis method has its own merits and demerits. For example, the solid-state reaction synthesis is clean but requires repeated grinding and high-temperature sintering, thus is quite time- and energy-consuming. The spray pyrolysis technique is suitable for mass production of oxide powders but suffers from intensive energy penalty. Comparatively, the sol–gel combustion synthesis route has attracted great interests for the production of homogeneous, high-purity oxide powders at significantly lower temperatures and less amount of external energy [4–10]. Further, the

*Corresponding author. Tel./fax: +86 22 83955663.
E-mail address: tanxiaoyao@tjpu.edu.cn (X. Tan).

0272-8842/$ - see front matter © 2013 Elsevier Ltd and Techna Group S.r.l. All rights reserved.
http://dx.doi.org/10.1016/j.ceramint.2013.07.004

synthesized oxide powders by the sol–gel combustion may retain their nanocrystalline structure even after sintering. However, this method has not received much commercial importance because a large amount of organic complexing agents such as ethylenediamine tetraacetic acid (EDTA) and/or citric acid is required for the production of the sols, leading to a noticeable increase in the process costs. Moreover, it also usually takes a long time to complete the complexing reaction so as to yield the pure perovskite phase.

Recently, a microwave-assisted combustion synthesis technique has been effectively used to produce spinel and fluorite ceramic powders [11–18]. In this synthesis process, the complexing reaction is achieved in a microwave oven, where heat is generated within the sample volume itself by the interaction of microwaves with the reactants. Unlike the conventional heating systems that heat the material from outer surface to interior resulting in steep thermal gradients, the microwave reactor can provide a uniform heating environment for the complexing reactions, leading to rapid formation of pure crystalline phase and sharply reducing the processing time and cost. Furthermore, the resultant oxide powders also exhibit small and uniform particle sizes (nano-powders), which is extremely useful in obtaining superior powder properties such as large surface area and high sinterability [19]. In this paper, the microwave-assisted sol–gel combustion was applied to synthesize nano-crystalline $Sm_{0.5}Sr_{0.5}Co(Fe)O_{3-\delta}$ (SSCF) perovskite oxides using glycine as the complexing agent. The synthesis conditions for the formation of pure perovskite structure have been investigated and optimized. The effect of Fe substitution for Co on the stability of the SSC perovskite against CO_2 has also been investigated by the XRD measurement.

2. Experimental

2.1. Powder synthesis

Metal nitrates $Sm(NO_3)_3 \cdot 6H_2O$ (99.95%, purity), $Sr(NO_3)_2$ (99.5% purity), $Co(NO_3)_2 \cdot 6H_2O$(99% purity), $Fe(NO_3)_3 \cdot 6H_2O$(98.5% purity) were used as the raw materials for metal ion sources. Glycine (NH_2CH_2COOH, 99.5% purity) and polyethylene glycol (PEG-2000, 99.5% purity) were used as the chelating agent and the dispersant, respectively. Metal nitrates were weighted according to the stoichiometry of the composite oxide and dissolved into deionized water in a glass beaker to form a mixed solution. A required amount of glycine and PEG-2000 (5 wt% of all the raw materials) were also dissolved into the mixed solution under stirring. The mole ratio of the total metal ions to glycine was controlled at 1:1, 1:1.5 or 1:2, while the gross metal ion concentration in the mixture was fixed at 0.12, 0.25 or 0.5 mol L^{-1}. The starting solution was placed in a microwave reactor (MCR-3, Tianjin Science and Technology Instrument Co, Ltd.) to perform complexing reaction at 80 °C with the stirring rate of 1000 r min^{-1}. As the excess water was evaporated continuously, the solution gradually turned into a viscous sol and in turn into a gel after 15–60 min depending on the initial concentration. The gel was then transferred to a 1000 mL pyrex beaker and moved into a microwave oven. After heating for around 2–5 min at 200 W power, auto-combustion of the gel took place to form the SSCF powder precursor. Further calcination of the oxide precursor was conducted at 600–1000 °C in static air for 2 h in a box-type furnace to remove the residual carbon and to form the desired perovskite structure.

2.2. Characterization

The morphology of the powders was observed using scanning electron microscope (SEM) (Hitachi S-4800, Japan). The powder samples were ultrasonically dispersed in ethanol prior to the measurement. Thermogravimetry/differential thermal analysis (TG-DTA) of the powder precursor was performed in a TG/DTA system (MDSC Q100, TA) with 10 °C min^{-1} scanning rate. Ten milligram powder precursor placed in a sample holder was heated from room temperature to 1200 °C in air with the flow rate of 50 mL min^{-1} while the weight and heat flux changes were recorded as a function of temperature. The specific surface area of the powders was measured using a surface area and porosimetry analyzer (TriStar 3000, Micromeritics Instrment Corp., USA) with N_2 as the adsorption gas. Based on the BET surface area values, the particle size of the powder was estimated by

$$d_{BET} = \frac{6}{\rho_{th} S_{BET}} \quad (1)$$

where S_{BET} is the BET surface area of the powder and ρ_{th} is the theoretical density of the SSC perovskite (6.834 g cm^{-3}).

The crystal structure of the powders was identified by X-ray diffractometer (Bruker D8 Advance, Germany) using CuKa radiation. Continuous scan mode was used to collect 2θ data from 20° to 80° with a 0.02° sampling pitch and a 2° min^{-1} scan rate. The X-ray tube voltage and current were set at 40 kV and 30 mA, respectively. From the X-ray diffractogram, the average crystallite size could be evaluated using the Scherrer equation,

$$d_{XRD} = \frac{0.9\lambda}{b \cos \theta} \quad (2)$$

where λ is the X-ray wavelength of CuKa radiation, $\lambda = 0.15418$ nm; θ is the diffraction angle (°); and b is the corrected half-width of the diffraction peak.

In order to measure the stability of the SSCF perovskite oxides, 20% CO_2–Ar mixture was passed to the powder samples, which were packed in a quartz tube located in a tubular furnace. After the treatment at 850 °C for 8 h, the powder samples were analyzed by XRD measurement to observe any changes in the crystalline structures.

3. Results and discussion

3.1. Morphology and crystal phase of the SSC powders

Fig. 1 displays the morphology of the SSC precursor and the oxide powders calcined at different temperatures. As can be seen from Fig. 1(a), the as-prepared SSC precursor demonstrated a

highly porous structure in which single particles could not be discriminated. After grinding and calcination at 600 °C for 2 h, the crystals/grains of the oxide powder in the size range of 30–50 nm have been observed clearly, as shown in Fig. 1(b). Agglomeration of the oxide particles occurred as a result of the decrease of surface energy by the grain contact and coalescence. These agglomerates could be easily broken into fine particles by a slight press. As the calcination temperature was increased to 800 °C, the crystals/grains of the oxide powder have grown up to 50–80 nm (Fig. 1(c)), which are much smaller than those obtained by the conventional combustion-synthesized route [6]. When the calcination temperature was further increased to 1000 °C, severe grain coalescence has taken place, resulting in the particle size to increase significantly up to 200–300 nm with the mean diameter of 223.60 nm, as shown in Fig. 1(d). The agglomeration and the particle growth also can be observed clearly by the measurement of the specific areas of the powders with the results summarized in Table 1. As can be seen, the BET area of the powder precursor was only 2.59 $m^2 g^{-1}$ with the estimated particle size of 339.1 nm. After ball-milling and calcination at 600 °C, the surface area of the powder got to 8.32 $m^2 g^{-1}$ with the corresponding particle size of 113.7 nm. However, the surface area would reduce with increasing the calcination temperature because of the particle growth. Furthermore, all the powder samples exhibited a much larger BET diameter than the SEM diameter value, indicating agglomeration has occurred. Therefore, it may be rationally concluded that the calcination temperature should not be too high so as to retain the nano particle properties of the oxide.

Fig. 2 shows the TG-DTA curves of the SSC powder precursor. As can be seen, the TG curve demonstrates a three-stage weight-loss profile. The first stage of the TG profile with a span of 30 to 600 °C can be attributed to the loss of water and the burn-out of the carbon residual produced during the auto-combustion process. It gives an intensive exothermic peak at around 295 °C on the DTA curve. The second is a relatively rapid weight-loss stage accounting for about 10.5% as the temperature increases from 600 °C to 760 °C. This stage corresponds to the thermal decomposition of the formed carbonate intermediates as well as the nitrate residuals and the formation of the perovskite phase, yielding a corresponding endothermic peak at around 755 °C on the DTA curve. After the temperature was higher than 800 °C, the weight of the sample almost would retain constant even though the temperature was further increased to 1200 °C.

The crystalline phase development as a function of the calcination temperature is depicted by the XRD patterns in Fig. 3. It can be seen that the perovskite phase has not been formed in the SSC powder precursor. After the powder precursor was calcined at 600 °C for 2 h, some peaks attributing to perovskite have appeared on the XRD curve, but the intensity of

Table 1
Properties of the SSC powders calcined at different temperatures.

SSC sample	Crystallite size d_{XRD} (nm)	Crystallinity (%)	d_{SEM} (nm)	S_{BET} (m^2/g)	d_{BET} (nm)
Powder precursor	/	/	/	2.59	339.1
Calcined at 600 °C	/	/	45.64	8.32	113.7
Calcined at 800 °C	18.40	42.23	72.17	5.23	167.7
Calcined at 1000 °C	42.78	79.16	223.60	1.35	693.8

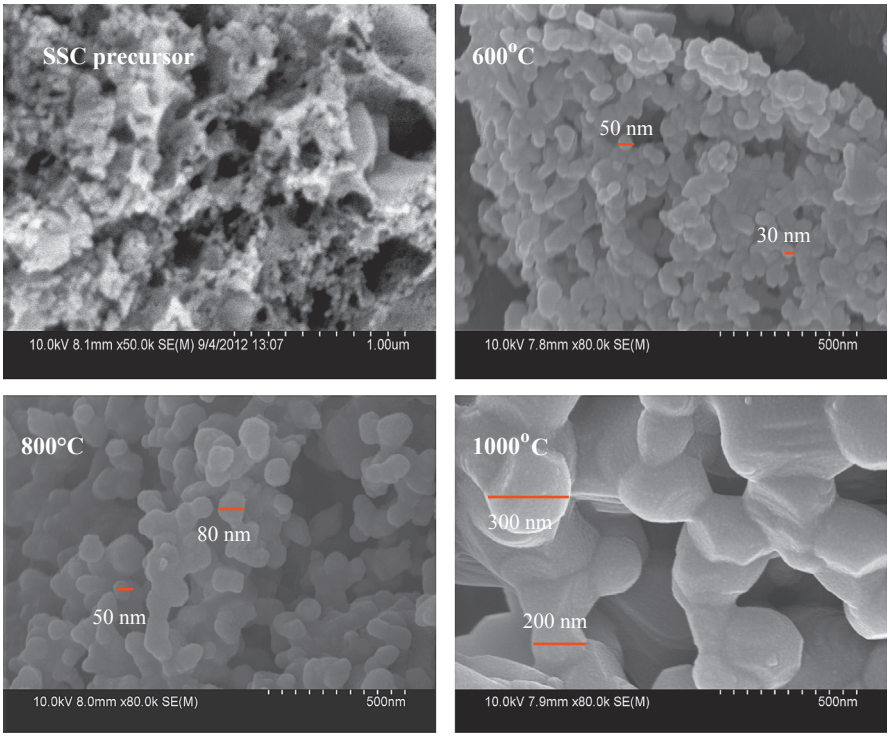

Fig. 1. Morphology of the SSC oxide precursor and the calcined powders at different temperatures.

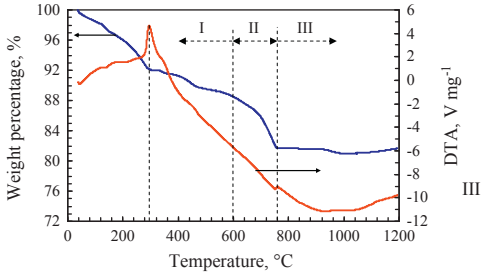

Fig. 2. TG-DTA curves of the SSC powder precursor.

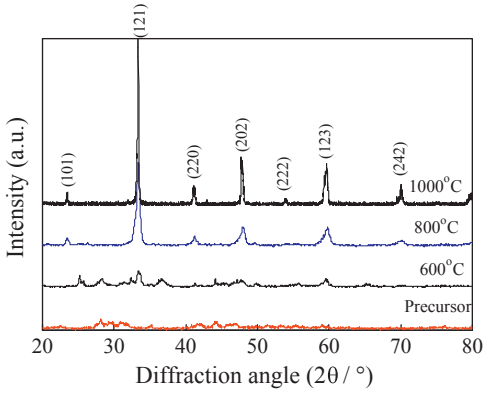

Fig. 3. XRD patterns of the SSC precursor and the oxide powders calcined at different temperatures.

these peaks are very low. This implies that the 600 °C calcined powder was actually a mixture of various metal oxides, carbonate salts, nitrates and some unknown intermediate phases. As the calcination temperature was increased to 800 °C, all the peaks have nearly disappeared except for those at the diffraction angles (2θ) of 23.35°{101}, 33.34°{121}, 40.98°{220}, 47.75°{202}, 53.86°{222}, 59.66°{123} and 70.02°{242}, which could be ascertained to be the characteristic peaks of the SSC orthorhombic perovskite phase (PDF reference code 53–0112). It means that the pure perovskite structure can be formed once the calcination temperature reaches 800 °C with a 2 h firing period. This is in good agreement with the result of the above TG-DTA measurement. By comparison, the single perovskite phase cannot be obtained in the conventional citrate complexation method until the calcination temperature reached up to 1100 °C, while the calcination temperature to form single perovskite phase for the freeze-drying method was 900 °C [6]. With the sintering temperature further increased to 1000 °C, the intensity of the characteristic peaks is noticeably enhanced, indicating that the perovskite crystals have grown up during the calcination at elevated temperatures. By means of the Scherrer's equation, the average crystallite sizes of the powders calcined at 800 °C and 1000 °C were calculated to be approximately 18.40 nm and 42.78 nm, respectively.

3.2. Effect of the glycine/metal-ion ratio

The amount of glycine relative to the metal ions is an important parameter for the synthesis of perovskite oxides since it not only functions as the complexing agent but also acts as the combustion agent in the sol–gel combustion process. If the amount of glycine used is not enough, it is difficult to ensure homogenous mixing of various metal ions and complete combustion of the finally formed gel, which will take negative effects on the formation of the pure perovskite phase. Fig. 4 shows the XRD patterns of the SSC powders synthesized using different glycine/metal-ion ratios, where all the samples were calcined at 1000 °C for 2 h. It can be seen that some impurity phases like $Sr_2Co_2O_5$ (PDF reference code 34-1475), $SrCO_3$ (PDF reference code 05-0418) and other unidentified phases are present in addition to the main perovskite phase in the SSC powder synthesized under the glycine/metal-ion ratio of 1:1. As the glycine/metal-ion ratio was increased, these impurity phases in the synthesized powders could be reduced or even removed completely. As can be seen from the figure, the SSC powder synthesized using 2:1 glycine/metal-ion ratio has demonstrated the pure perovskite phase although it was still calcined at 1000 °C for 2 h. Therefore, in order to obtain pure perovskite oxides with high economical efficiency, the glycine/metal-ion ratio used in the microwave-assisted sol-gel combustion process should be controlled to be around 2:1.

3.3. Effect of the metal-ion concentration

Fig. 5 shows the XRD patterns of the SSC powders synthesized with different metal ion concentrations in the starting solutions. As can be seen, all the three synthesized powders have exhibited the pure perovskite structure but the sample derived by the 0.5 mol L^{-1} starting concentration demonstrated relatively lower crystallization intensity. This implies that the starting metal ion concentration takes little effect on the formation of the perovskite structure. Note that a lower starting concentration may lead to longer complexing reaction time. For example, it was found that the time to complete the complexing reaction would increase from around 15 min to 60 min when the starting metal ion concentration decreased from 0.5 mol L^{-1} to 0.12 mol L^{-1}. In order to obtain the pure perovskite oxides with less time but high crystallization, the gross metal ion concentration in the starting solution should be controlled at around 0.25 mol L^{-1}, with which the complexing reaction time is around 30 min. It also indicates that the synthesis time can be significantly reduced with the help of the microwave heating technique.

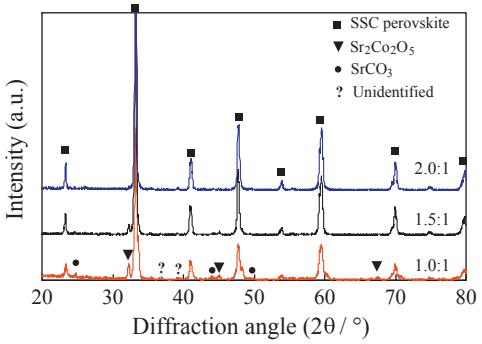

Fig. 4. XRD patterns of the SSC powders synthesized under different glycine/metal-ion ratios (all samples were calcined at 1000 °C for 2 h).

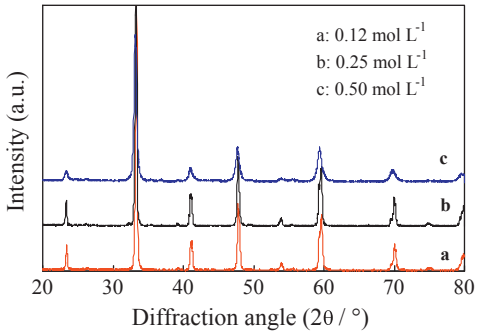

Fig. 5. XRD patterns of the SSC powders prepared with different starting metal ion concentrations (all samples were calcined at 1000 °C for 2 h).

3.4. Effect of Fe-doping on the perovskite stability

Fig. 6 compares the XRD patterns of the SSC, $Sm_{0.5}Sr_{0.5}Co_{0.4}Fe_{0.6}O_{3-\delta}$ (SSCF0.6) and $Sm_{0.5}Sr_{0.5}FeO_{3-\delta}$ (SSF) powders calcined at 1000 °C for 2 h. It can be seen that the perovskite structure of the oxides has not been changed after the substitution of Fe for Co cations. However, the characteristic peaks would shift gradually to the low angle direction with increasing the doping content of Fe ions in the composition. For example, the {121} peaks for the SSC, SSCF0.6 and SSF perovskites appeared at (2θ) 33.28°, 33.00° and 32.70°, respectively. This is because the substitution of Co^{3+} (0.0610 nm) cation with the bigger Fe^{3+} (0.0645 nm) cations has led to the lattice expansion of the perovskite cell [9]. With the help of MDI Jade 5.0 software, the cell parameters of the SSCF oxides at room temperature were given as (a × b × c) 0.53663 nm × 0.75932 nm × 0.53740 nm for SSC, 0.53855 nm × 0.76482 nm × 0.53733 nm for SSCF0.6 and 0.54948 nm × 0.77583 nm × 0.54962 nm for SSF. Furthermore, some additional small peaks have appeared on the XRD pattern of the SSF oxide, indicating some impurity phases were present in the SSF composite although it was calcined at 1000 °C. The deep analysis performed using MDI Jade 5.0 software showed that these impurities were mainly Fe-compounds like $SmFeO_3$ (PDF reference code 08–0149), $SrFe_{12}O_{19}$ (PDF reference code 33–1340) and FeO (PDF reference code 49–1447). This also indicated that a higher calcination temperature is usually required in order to obtain the pure perovskite structure for those Fe-doped oxides.

It is known that the substitution of Fe for Co in SSC may reduce the thermal expansion coefficient (TEC) of the perovskite so as to match the expansion of the electrolyte in SOFCs, but also resulting in the decrease in electrical conductivity [20]. Our present work mainly focused on the perovskite stability especially in the CO_2-containing atmosphere. Fig. 7 shows the XRD patterns of the SSC, SSCF0.2 and SSCF0.4 powders after exposing to the 20% CO_2–Ar atmosphere at 850 °C for 8 h. As can be seen, both the SSCF0.2 and SSCF0.4 oxides have preserved the perovskite structure well except that a small impurity peak occurred at (2θ) 32.82° on the XRD curve of the SSCF0.2 oxide. However, sever phase degradation took place in the SSC powder after the CO_2 exposure, forming degradation products such as $Sr_2Co_2O_5$, $SrCO_3$ and Co_3O_4 (PDF reference code 42–1467), as can be clearly seen on the XRD pattern.

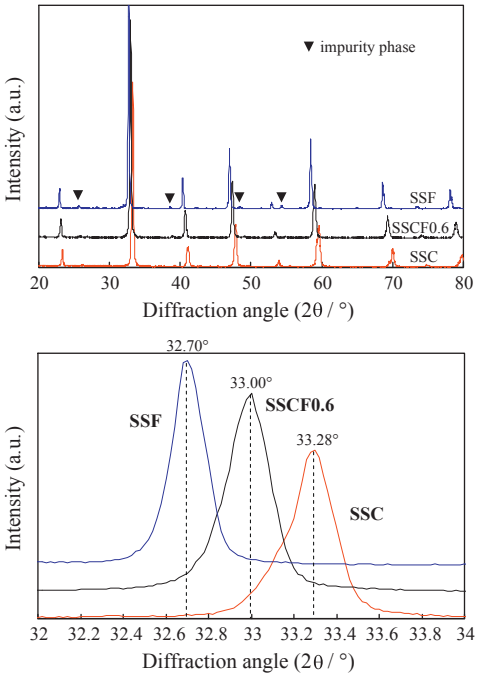

Fig. 6. XRD patterns of the SSC, SSCF0.6 and SSF powders calcined at 1000 °C.

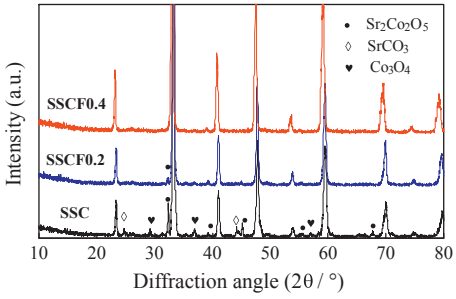

Fig. 7. Stability of the SSCFx perovskites in the CO_2-containing atmosphere (850 °C; 20% CO_2–Ar mixture feed; exposure time = 8 h).

Therefore, an appropriate substitution of Co with Fe ions ($x > 0.2$) can improve significantly the stability of the perovskite structure of the oxide against CO_2. It implies that the Fe doped SSCF perovskite may be a good CO_2-resistant membrane material for oxygen permeation.

4. Conclusion

Nano crystalline $Sm_{0.5}Sr_{0.5}Co(Fe)O_{3-\delta}$ perovskite oxides have been synthesized via the microwave-assisted sol–gel process. In order to obtain the pure perovskite structure with improved economical efficiency, the glycine/metal-ion ratio in the starting solution should be controlled at about 2 with the metal ion concentration of 0.25 mol L^{-1} and the calcination temperature to be around 800 °C. The synthesis period can be significantly reduced by using the microwave heating technique. The partial substitution of Fe for Co cations with a molar fraction of higher than 0.2 could improve the stability of the perovskite against CO_2 significantly, but the calcination

temperature to form pure perovskite phase should also be increased to some extent.

Acknowledgments

The authors gratefully acknowledge the research funding provided by the National Natural Science Foundation of China (NNSFC 21176187), Tianjin Research Program of Application Foundation and Advanced Technology (11JCZDJC23400).

Appendix A. Supporting information

Supplementary data associated with this article can be found in the online version at http://dx.doi.org/10.1016/j.ceramint.2013.07.004.

References

[1] J. Sunarso, S. Baumann, J.M. Serra, W.A. Meulenberg, S. Liu, Y.S. Lin, J.C.D. da Costa, Mixed ionic-electronic conducting ceramic-based membranes for oxygen separation, Journal of Membrane Science 320 (2008) 13–41.

[2] H.J.M. Bouwmeester, Dense ceramic membranes for methane conversion, Catalysis Today 82 (2003) 141–150.

[3] H.T. Giang, H.T. Duy, P.Q. Ngan, G.H. Thai, D.T.A. Thu, D.T. Thu, N.N. Toan, Hydrocarbon gas sensing of nano-crystalline perovskite oxides LnFeO3 (Ln=La, Nd and Sm), Sensors and Actuators B 158 (2011) 246–251.

[4] X. Meng, B. Meng, X. Tan, N. Yang, Z. Ma, Synthesis and properties of $Ba_{0.5}Sr_{0.5}Co_{0.6}Zr_{0.2}Fe_{0.2}O_{3-\delta}$ perovskite cathode material for IT-SOFCs, Materials Research Bulletin 44 (2009) 1293–1297.

[5] F. Wang, D. Chen, Z. Shao, $Sm_{0.5}Sr_{0.5}CoO_{3-\delta}$-infiltrated cathodes for solid oxide fuel cells with improved oxygen reduction activity and stability, Journal of Power Sources 216 (2012) 208–215.

[6] L.M. Acuna, J. Pena-Martínez, D. Marrero-López, R.O. Fuentes, P. Nunez, D.G. Lamas, Electrochemical performance of nanostructured $La_{0.6}Sr_{0.4}CoO_{3-\delta}$ and $Sm_{0.5}Sr_{0.5}CoO_{3-\delta}$ cathodes for IT-SOFCs, Journal of Power Sources 196 (2011) 9276–9283.

[7] H. Ding, X. Xue, X. Liu, G. Meng, High performance protonic ceramic membrane fuel cells (PCMFCs) with $Sm_{0.5}Sr_{0.5}CoO_{3-\delta}$ perovskite cathode, Journal of Alloys and Compounds 494 (2010) 233–235.

[8] F. Dong, D. Chen, R. Ran, H. Park, C. Kwak, Z. Shao, A comparative study of $Sm_{0.5}Sr_{0.5}MO_{3-\delta}$ (M=Co and Mn) as oxygen reduction electrodes for solid oxide fuel cells, International Journal of Hydrogen Energy 37 (2012) 4377–4387.

[9] J. Gao, X. Song, F. Zhou, S. An, Y. Tian, Substituent effects of Ba^{2+} for Sm^{3+} on the structure and electrochemical performances of $Sm_{0.5}Sr_{0.5}Co_{0.8}Fe_{0.2}O_{3-\delta}$ cathode for intermediate temperature solid oxide fuel cells, Journal of Power Sources 218 (2012) 383–392.

[10] Q. Feng, X.H. Ma, Q.Z. Yan, C.C. Ge, Preparation of soft-agglomerated nano-sized ceramic powders by sol–gel combustion process, Materials Science and Engineering B 162 (2009) 53–58.

[11] I. Ganesh, R. Johnson, G.V.N. Rao, Y.R. Mahajan, S.S. Madavendra, B.M. Reddy, Microwave-assisted combustion synthesis of nanocrystalline $MgAl_2O_4$ spinel powder, Ceramics International 31 (2005) 67–74.

[12 Y.-P. Fu, Y.-H. Su, C.-H. Lin, S.-H. Wu, Comparison of the microwave-induced combustion and solid-state reaction for the synthesis of $LiMn_2O_4$ powder and their electrochemical properties, Ceramics International 35 (2009) 3463–3468.

[13] Y.-P. Fu, C.-H. Lin, Preparation of Y_2O_3-doped CeO_2 nanopowders by microwave-induced combustion process, Journal of Alloys and Compounds 389 (2005) 165–168.

[14] Y.-P. Fu, C.-H. Lin, K.-Y. Pan, Microwave-induced combustion synthesis of yttrium iron garnet nano-powders and their characterizations, Journal of Magnetism and Magnetic Materials 272–276 (2004) 2202–2204.

[15] H. Mohebbi, T. Ebadzadeh, F.A. Hesari, Synthesis of nano-crystalline NiO-YSZ by microwave- assisted combustion synthesis, Powder Technology 188 (2009) 183–186.

[16] Y.-P. Fu, C.-H. Lin, C.-W. Liu, K.-W. Tay, S.-B. Wen, Microwave-induced combustion synthesis and electrical properties of $Ce_{1-x}Sm_xO_{2-1/2x}$ ceramics, Journal of Power Sources 159 (2006) 38–41.

[17] L. Combemale, G. Caboche, D. Stuerga, D. Chaumont, Microwave synthesis of yttria stabilized zirconia, Materials Research Bulletin 40 (2005) 529–536.

[18] R.V. Mangalaraja, J. Mouzon, P. Hedström, C.P. Camurri, S. Ananthakumar, M. Odén, Microwave assisted combustion synthesis of nanocrystalline yttria and its powder characteristics, Powder Technology 191 (2009) 309–314.

[19] N.P. Bansal, Z. Zhong, Combustion synthesis of $Sm_{0.5}Sr_{0.5}CoO_{3-x}$ and $La_{0.6}Sr_{0.4}CoO_{3-x}$ nanopowders for solid oxide fuel cell cathodes, Journal of Power Sources 158 (2006) 148–153.

[20] H. Lv, Y. Wu, B. Huang, B. Zhao, K. Hu, Structure and electrochemical properties of $Sm_{0.5}Sr_{0.5}Co_{1-x}Fe_xO_{3-\delta}$ cathodes for solid oxide fuel cells, Solid State Ionics 177 (2006) 901–906.